J Vis (2010) 13:33–40
DOI 10.1007/s12650-009-0009-2

REGULAR PAPER

Harald Kleine · Cuong Vo Le · Kohsei Takehara · T. Goji Etoh

Time-resolved visualization of shock–vortex systems emitted from an open shock tube

Received: 21 April 2009 / Revised: 29 August 2009 / Accepted: 3 September 2009 / Published online: 12 December 2009
© The Visualization Society of Japan 2009

Abstract When a shock wave leaves an open-ended shock tube, it generates a vortex ring that subsequently detaches from the shock tube and follows the expanding shock front. This classical problem of shock–vortex interaction has been visualized in unprecedented detail and temporal resolution by means of time-resolved shadow, schlieren and shearing interferometry sequences obtained with a newly developed ultrahigh-speed color video camera. This device is capable of taking 144 frames with full-frame resolution of 720 × 410 pixels at rates of up to one million frames per second. Apart from shadowgraphy, the visualization techniques used in this study were direction- and magnitude-indicating color schlieren and polychrome shearing interferometry. The process was observed both with the standard normal view of the flow field and with an oblique view, which facilitated the identification of some three-dimensional flow features. The obtained results clearly show the development of individual flow elements, including some that so far have eluded a proper description. One example is the secondary, counter-rotating vortex ring, which at a later time wraps around the main vortex ring before disintegrating upon merging with the shear layer that surrounds the gas exiting from the tube.

Keywords Shock–vortex interaction · High-speed camera · Shadowgraphy · Schlieren · Shearing interferometry

1 Introduction

When a shock wave emanates from an open shock tube into the surrounding atmosphere, it creates a complex flow field the primary components of which are the expanding shock followed by a vortex ring and a jet of gas exiting the tube. This relatively simple and straightforward test configuration has been investigated for several decades, partially because it is related to studies of noise generation through the interaction of shock waves and compressible vortices (e.g., Chang and Chang 2000). The first systematic study of the process, including its visualization through schlieren spark photography, is attributed to Elder and de Haas (1952). This and most subsequent experimental studies have visualized the process by means of single-image high-speed photography, where the recording medium is exposed by a single short-duration flash of light. The temporal development of the process is then assembled from several records obtained in different

H. Kleine (✉)
School of Aerospace, Civil and Mechanical Engineering, University of New South Wales/Australian Defence Force Academy, Northcott Drive, Canberra, ACT 2600, Australia
E-mail: h.kleine@adfa.edu.au
Tel.: +61-2-62688047
Fax: +61-2-62688276

C. Vo Le · K. Takehara · T. G. Etoh
Department of Civil Engineering, Kinki University, 3-4-1, Kowakae, Higashi-Osaka 577-8502, Japan

experiments with identical initial conditions. A notable exception is a test conducted with the Cranz-Schardin camera (Oertel 1966), where multiple spark sources were fired in a predetermined sequence to provide a time-resolved shadowgraph series of the process in a single experiment. More recently, Kainuma et al. (2005) used a high-speed video camera to study the influence of the shape of the shock tube outlet on the formation and propagation of the vortex ring. Their study concentrates, however, on the low Mach number regime in which the flow exiting the shock tube remains subsonic and the vortex is free of discontinuities. In contrast to this, the present paper describes an investigation of the formation of the vortex ring and its embedded discontinuities in the case of a supersonic outflow from the tube. This is, to the best of the authors' knowledge, the first time that this process has been visualized in true time-resolved fashion with imaging frequencies of up to several hundred kilohertz and a suite of different visualization techniques.

The vortex ring typically generates a strong signal that can easily mask the traces of other weaker flow features. Therefore, several different visualization techniques were used, to highlight different aspects of the flow. Techniques that are primarily detecting density changes perpendicular to the flow direction, such as shearing interferometry with horizontal fringe alignment or a schlieren method with a horizontal cutoff, "ignore" the strong density gradients of most parts of the vortex ring. Such methods can therefore be used to investigate details of the flow at the center of the vortex ring.

2 Experimental setup

2.1 Test facility and visualization system

The tests were conducted with a cylindrical shock tube that had an inner diameter of 20 mm and an overall length of 2.65 m, of which the low pressure part occupied 1.65 m. The test gas was ambient air and the driver gas compressed air at pressures between 0.15 and 0.6 MPa, depending on the thickness of the Mylar diaphragm that separated the sections. Tests were run either by pressurizing the high-pressure part until a natural rupture of the diaphragm occurred, or by activating a needle plunger at a fixed overpressure. The obtained shock Mach number M_S was repeatable within a margin of ± 0.02. The shock Mach numbers tested in these experiments ranged from 1.1 to 1.6, with the majority of tests conducted at a nominal shock Mach number of $M_S = 1.4$.

The basic scheme for density-sensitive visualization of this process is largely analogous to the systems used in other studies (e.g., Elder and de Haas 1952; Minota et al. 1997), except that these previous studies used only shadowgraphy and monochrome schlieren techniques for single-image visualization. Here, a Z-type schlieren system with two spherical mirrors of 3 m focal length and 300 mm diameter was combined with the high-speed video camera described in Sect. 2. The used schlieren technique is known as the dissection method introduced by Cords (1968). In this system, a source mask with a color filter arrangement and a corresponding cutoff device are placed in the focal planes of the first and second mirror, respectively, as indicated in Fig. 1. When the direction-indicating color schlieren method is used, a cylindrical lens is required to correct the inherent astigmatism of the apparatus. Extensive descriptions of the principle layout of these optical systems are given in, e.g., Settles (2001), Kleine (2001). By removing the cutoff device and changing the source mask to a simple pinhole, the system converts into an imaging shadowgraph apparatus. Usually this conversion also involves a change of position of the imaging lens, to image the shadow plane rather than the object itself. If both source mask and cutoff device are replaced by a polarizer/Wollaston prism combination, the optical system becomes a shearing interferometer (Kleine 2001; Merzkirch 1987). The light source in each case is a powerful photography flash unit (Metz Mecablitz CT45) that can deliver intense light for about 1 ms. The light source and the camera are triggered by the shock wave via one of two pressure transducers located close to the tube exit. These transducers are also used to measure the time-of-flight of the shock which yields, with an additional measurement of ambient temperature, its Mach number.

Simultaneous front lighting of the tube exit is achieved with the help of a second identical powerful flash unit. The use of front lighting exploits the fact that the portion of the visualization system behind the test section can be considered as a simple imaging unit; if the object is illuminated from the camera side of the setup, an image of the object is created simultaneously with the image of the flow. Hence the object does no longer appear simply as a dark silhouette but is properly imaged with usually sufficient indication of its spatially distributed components (Kleine et al. 2008). Such front lighting is useful in the case of schlieren and shearing interferometry techniques, but cannot be applied for shadowgraphs as in this visualization system the imaging lens typically does not focus on the object but on the shadow plane. In this case, the

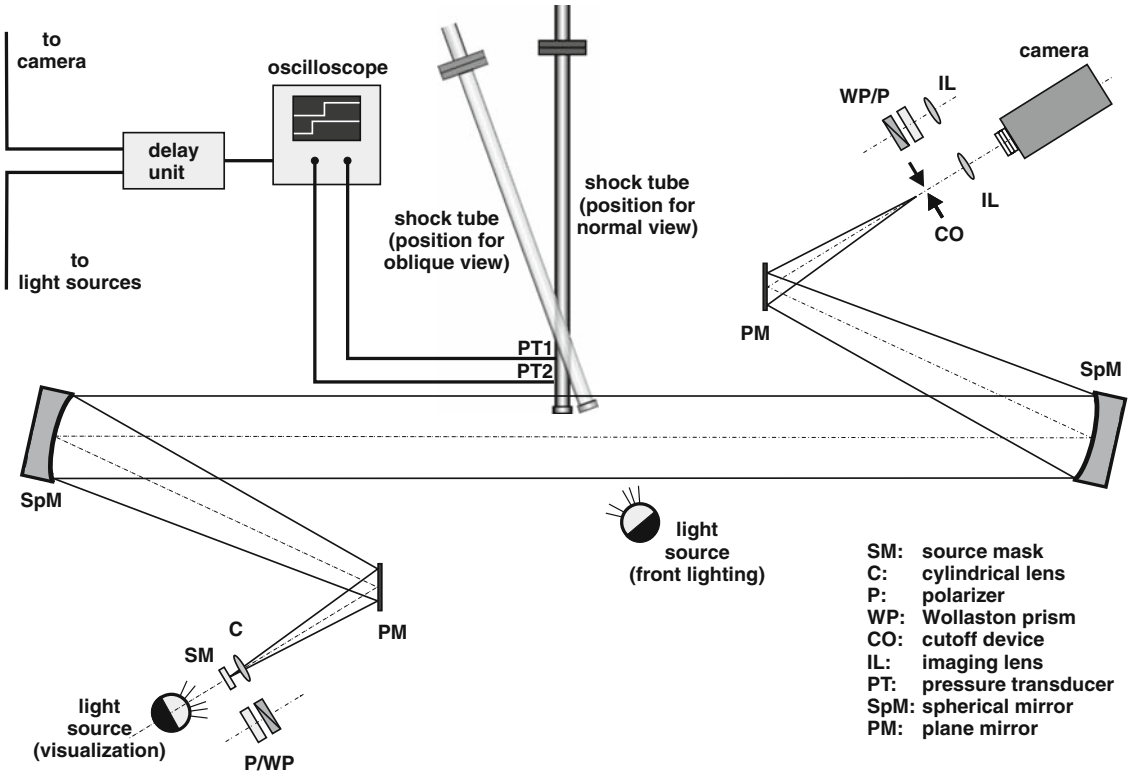

Fig. 1 Schematic sketch (not true to scale) of experimental setup

front lighting would accentuate the deliberate defocusing, which in general is detrimental to the overall image. A strong light source is needed to provide sufficient diffusely reflected light from the front-lit object. To avoid specular reflection and to obtain an even illumination of the front-lit shock tube exit, its outer surface was mildly sandblasted to give it an overall matt finish.

In typical density-sensitive visualization systems, the visualizing beam passes perpendicularly through the flow field, which in most cases is confined by test section windows. In the case of shock waves exiting from an open shock tube this constraint does not exist and it is possible to visualize the flow from different angles. For a test setup like the one described here, one usually rotates the shock tube while leaving the visualization system unchanged, as indicated in Fig. 1. Such images were already obtained by Elder and de Haas (1952) and in many of the subsequent investigations, but usually without the aforementioned front lighting. It is this front lighting that enhances the striking three-dimensional appearance of the resulting images, especially in schlieren visualizations. It has to be remembered, however, that the resulting image of the flow is always a projection and therefore carries no inherent three-dimensional information. The three-dimensional impression of some flow elements is partially caused by a characteristic feature of schlieren techniques, namely to represent density variations of a transparent, non-reflecting medium in the same way that height variations of a diffusely illuminated reflecting surface are displayed (Kleine and Settles 2008). The imaging of solid objects in the flow as diffusely reflecting surfaces—as it is achieved by front lighting—enhances the impression of three-dimensionality of the visualized flow, which is, however, to a large extent an optical illusion (Kleine et al. 2008). Nonetheless, significant new information about the flow can be gained from such oblique views. In the tests shown here, the tube was rotated approximately by 24° for the oblique view.

2.2 Camera

The time-resolved visualization of the shock wave processes which is briefly outlined in Sect. 1 was conducted with an ultrahigh-speed high-sensitivity color video camera prototype of 300,000 pixels, which was developed by NHK (Ohtake et al. 2006). The camera has a special CCD image sensor that uses an in-situ storage image sensor (ISIS) structure, invented by Etoh et al. (2002), allowing image capturing with up

to 1,000,000 frames per second (fps) at full-frame resolution. This frame rate is more than sufficient for the present study which requires primarily a large frame number, good spatial resolution and polychrome recording capability. Other camera systems, such as image converter cameras can operate at higher frame rates, but are inevitably monochrome and have significantly fewer frames, and were therefore not considered for this investigation. Similarly, current CMOS-based video systems cannot achieve the frame rates at the image resolution needed for this investigation.

Details on the principle of the camera used in these tests and the structure of its ISIS sensor can be found in Refs. (Ohtake et al. 2006; Etoh et al. 2002). The relevant specification data for the operation of the camera are given in Table 1. The four-phase transfer CCD camera is able to operate at a maximum frame rate of 1,000,000 fps without a decrease of resolution. The charge capacity and the noise level are about 11,500 electrons and 10 electrons, respectively, resulting in a 10 bit dynamic range. A color filter is incorporated into the image sensor chip. The imaging area fits within a circle of 41.8 mm diameter, which allows one to install a standard F-mount lens. In the optical system used here, however, the imaging lens must have a large focal length (>500 mm) and a correspondingly large distance from the sensor in order to achieve the desired image magnification. Therefore, instead of a standard camera lens a regular achromatic doublet is used.

The camera has two operating modes, namely a continuous overwriting mode and a continuous readout mode. For the experiment, the former was used with a total number of 144 recorded frames, which is sufficient for capturing high-speed phenomena in various scientific fields.

2.2.1 Continuous overwriting mode

Signals from each photodiode are simultaneously transferred to the in-situ linear CCD memories and continuously drained at the end to the outside of the sensor. The parallel recording operation at all pixels provides the ultimate high frame rate. The continuous overwriting mode allows the latest image signals to be stored in the linear CCD memory. When a target event is detected, a trigger signal is generated to stop the overwriting mode. Subsequently, image signals stored in the linear CCD memory inside the sensor are gradually transferred to and stored in an external memory.

2.2.2 Continuous readout mode

A 16-channel parallel readout scheme is employed in this camera to attain continuous image capture at a frame rate as high as 1,000 fps. Image signals are sequentially stored in the external memory until storage capacity is reached.

3 Results and discussion

3.1 Starting process

The first 350 μs of the process is shown in Fig. 2, visualized with the help of five different density-sensitive visualization techniques. Direct comparison of corresponding frames clearly shows that each technique highlights different features of the process. It also becomes obvious that some flow elements can be easily overlooked if one resorts only to a single visualization method.

Table 1 Specifications of high-speed camera

Image sensor	Ultrahigh-speed CCD
Resolution	720 pixels (H) × 410 pixels (V)
Frame rate	30 to 1,000,000 fps (continuous overwriting mode) 30 to 1,000 fps (continuous readout mode)
Pixel size	50.4 μm × 50.4 μm (2,540.2 μm^2)
Optical fill factor	16% (406.4 μm^2)
Dynamic range	10 bit
Transfer scheme	4-Phase transfer
Color filter	RGB (Bayer type)
Video output	HD-SDI:1
External trigger input	TTL or switch closure
Lens mount	F-mount

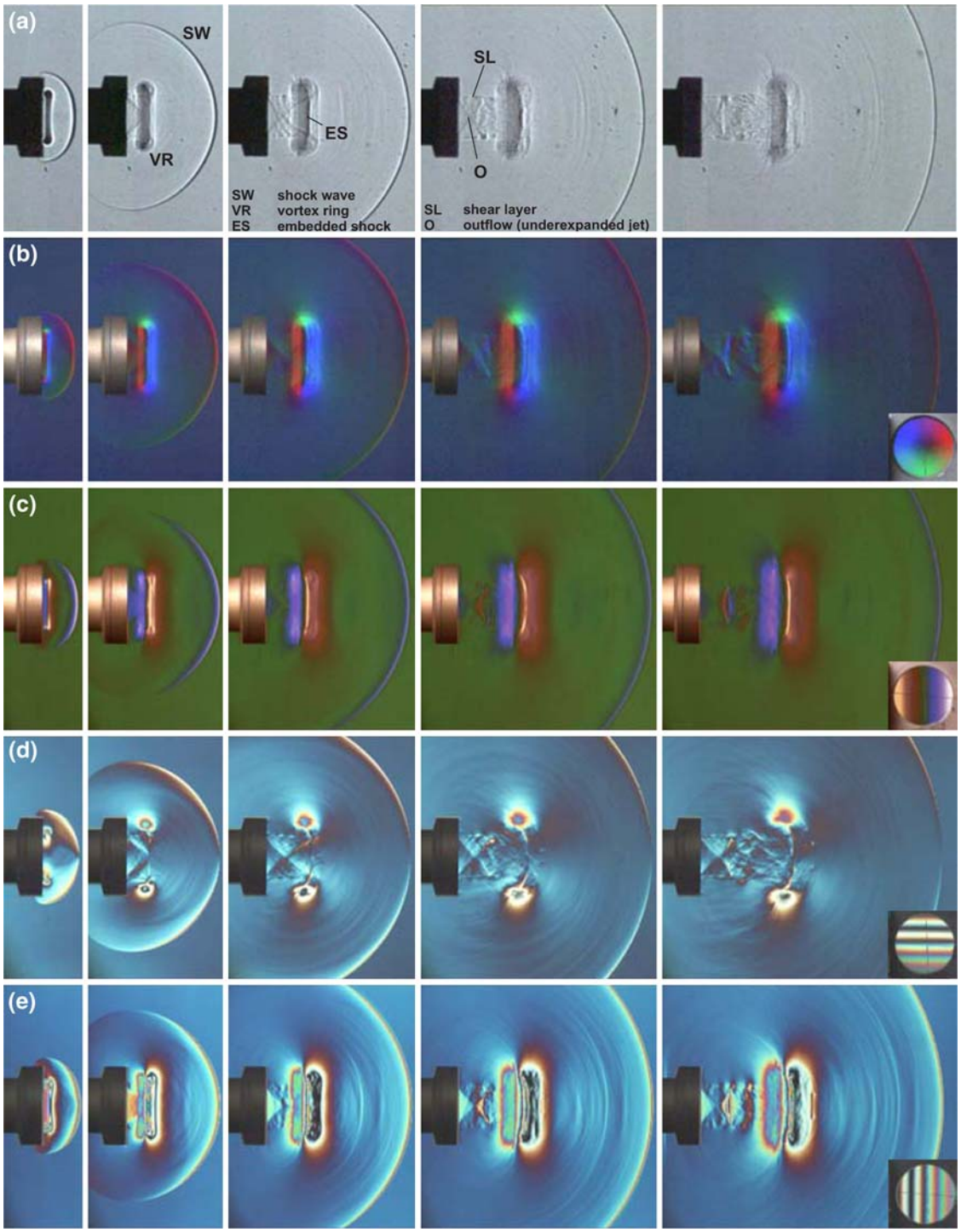

Fig. 2 Visualization of a shock wave (nominal M_S = 1.4) exiting from an open-end tube; selected frames from time-resolved sequences taken with 145,000 fps; Δt between shown adjacent frames: 69 μs; insets in **b**–**e** show the calibration image that displays the correlation between recorded color and encountered density gradient (see Kleine (2001) for details); exposure time of each frame: 0.86 μs; **a** shadowgraph; **b** direction-indicating color schlieren; **c** magnitude-indicating color schlieren (*vertical cutoff*); **d** shearing interferometry (*horizontal fringes*); **e** shearing interferometry (*vertical fringes*)

The initial shock wave diffracts at the edge of the tube upon exiting into the ambient atmosphere. The main features of this process are largely identical to what is observed for the diffraction of a plane shock wave at a 90° corner (Skews 1967; Kleine et al. 2003). The planar diffraction process is schematically

shown in Fig. 3. The transmitted diffracted shock DS weakens with increasing angle to the tube axis, which is clearly visible in all first frames of Fig. 2, and an expansion wave EW propagates upstream back into the tube. The flow set into motion by the initial shock wave is subjected to two different processes: downstream, outside of the tube, it cannot follow the rapid area expansion and detaches from the edge of the tube, with the resulting shear layer rolling up and forming the vortex V. Upstream, the flow undergoes an unsteady acceleration caused by the expansion wave that is moving back into the tube. As a result, the outflow from the tube becomes supersonic, even when the flow set into motion by the initial shock is far from the sonic limit. One-dimensional shock wave theory predicts that for diatomic gases the shock Mach number must exceed $M_S = 2.07$ to obtain supersonic speed behind the shock, but the unsteady expansion lowers this threshold to $M_S \approx 1.35$ in the planar case (Kleine et al. 2003; Sun and Takayama 1997). In the present axisymmetric case this threshold is seen to be even lower as the annular geometry enhances the acceleration. In contrast to the planar case, which can be treated as a self-similar problem without a characteristic length scale, the dimensions of the tube become important parameters in the case of an axisymmetric shock diffraction. The overall unsteady acceleration of the flow in the tube depends on how quickly the annular expansion wave generated at the circular corner combines to a planar expansion front and hence the occurrence of a supersonic flow will be influenced by the diameter of the tube. Once the outflow is established, its pattern is that of an underexpanded jet—at the tube exit, the pressure is higher than the surrounding ambient pressure, and a steady expansion wave centered at the edge of the tube is required to adjust the flow pressure to that of the environment.

Shortly after the first local supersonic flow patches are generated as a result of the unsteady expansion, secondary shock waves SSW appear on the top of the rolling-up shear layer. They adjust flow velocity and pressure between the accelerated outflow from the tube and the decelerated flow behind the expanding diffracted shock wave (Skews 1967; Kleine et al. 2003). In the axisymmetric case, these waves are partially obscured by the vortex ring, but they eventually combine and become visible in the form of an embedded shock within the vortex slightly ahead of its core. The present results give clear evidence for this interpretation of the development of the shock within the vortex and thus provide a correction of the widely accepted description of the starting process in (Baird 1987).

3.2 Secondary vortex ring

The secondary shock waves are initially small discontinuities that form on the top of the rolling up shear layer. With time, they grow and begin to coalesce until they eventually become the aforementioned shock embedded in the vortex. During the coalescence process, the interaction of secondary shocks from different parts of the vortex ring leads to the formation of an annular shear layer, which is convected further downstream to the front face of the vortex ring (see Fig. 2d, third frame, and Fig. 4). This shear layer rolls up to become a narrow, counter-rotating secondary vortex ring, formed at the front face of the main vortex ring (see the last two frames of each visualization in Fig. 2, in particular, Fig. 2e). This narrow vortex was already observed by Brouillette and Hébert (1997) and by Minota (1998), but the single-image visualizations of their studies could not reveal the development of this flow element.

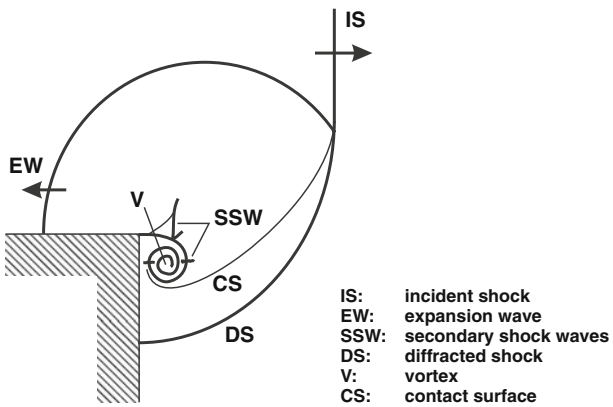

Fig. 3 Schematic of the flow features of plane shock wave diffraction at a 90° corner (adapted from Kleine et al. (2003))

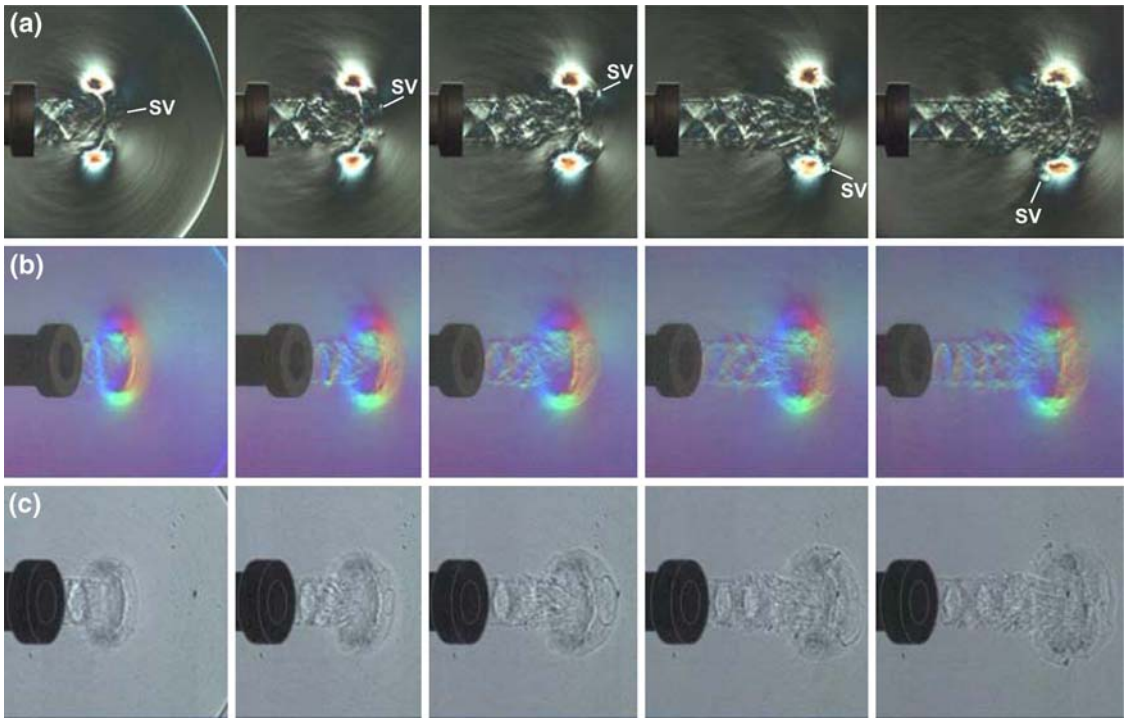

Fig. 4 Development of the secondary vortex (SV) ahead of the vortex ring generated by a shock wave exiting from an open-end tube (nominal M_S = 1.4); selected frames from time-resolved sequences taken with 145,000 fps; Δt between shown adjacent frames: 69 μs; exposure time of each frame: 0.86 μs; **a** shearing interferometry (normal view, *horizontal fringes*); **b** direction-indicating color schlieren (*oblique view*); **c** shadowgraph (*oblique view*; tube contours delineated after recording)

Oblique view visualizations confirm the initially annular structure of this feature (Fig. 4b, c). The annular symmetry is increasingly distorted when the main vortex ring forces the narrow secondary vortex to expand outward and wrap around the main vortex ring to give the latter the appearance of a mushroom cap (Fig. 4, last frames of a–c). The secondary vortex maintains its narrow and well-defined core and only disintegrates when it merges with the boundary of the supersonic jet. A single narrow vortex is only seen for relatively low shock Mach numbers, namely for the regime in which the secondary shocks have just started to appear (approx. $1.35 < M_S < 1.45$) and where their merging leads to an only mildly disturbed shear layer. For higher initial shock Mach numbers, the interaction of the secondary shocks is stronger, and the resulting shear layer breaks up into several vortices rather than only one (see Fig. 5). These vortices have typically a less well-defined core and tend to merge into a larger vortical structure when they are convected around the main vortex ring (Fig. 5, last frame). To visualize the details of the initial formation of the vortex, shearing interferometry with horizontal fringe alignment is highly suitable as it is capable of removing the strong signal generated by the main vortex ring while being sensitive enough to detect the details of the jet outflow (Figs. 2d and 4a).

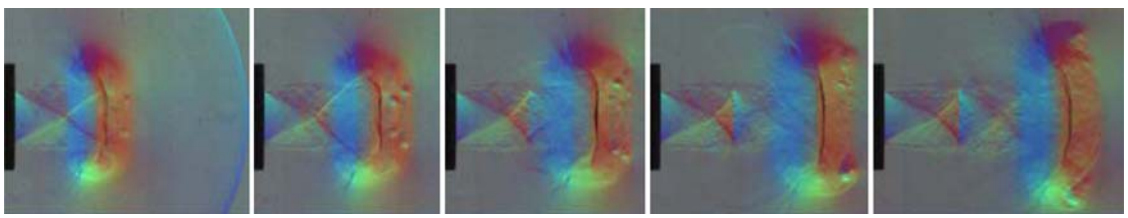

Fig. 5 Development of multiple secondary vortices ahead of the vortex ring generated by a shock wave (M_S = 1.56) exiting from an open-end tube; selected frames from a time-resolved direction-indicating color schlieren sequence taken with 210,000 fps; Δt between shown adjacent frames: 47.6 μs; exposure time of each frame: 0.6 μs

4 Summary and conclusions

The unsteady process of a shock wave exiting an open shock tube has been visualized, for the first time, in true time-resolved fashion by means of a suite of density-sensitive visualization techniques and a new ultrahigh-speed color video camera. While most of the flow features that could be observed in the present time-resolved sequences had already been detected in earlier research, their origin and their development have become obvious only now through this study, in which the process could be investigated in unprecedented temporal and spatial resolution with the help of a set of advanced flow visualization methods. These visualizations revealed previously unavailable details of the starting process, which was seen to display elements similar to those of the planar shock diffraction case. Secondary shock waves develop on top of the rolling up shear layer, and later they coalesce to form a shock embedded in the vortex. The interaction of these waves during coalescence gives rise to the formation of a secondary, narrow counter-rotating vortex ring, which is then transported outward by the main vortex ring before eventually disintegrating in the boundary of the supersonic jet.

A full analysis of the results to develop quantitative criteria to predict the onset and development of some flow features is still ongoing. While other visualization methods, such as reference beam interferometry and other means of investigation, such as CFD are required to fully quantify the process, the present results already demonstrate clearly the value of true time-resolved visualization as well as the advantage of using multiple visualization techniques.

Acknowledgments We would like to acknowledge the excellent technical support provided by Mr. Michael Jones of UNSW@ADFA, who designed and manufactured crucial parts of the shock tube used in these tests. We are also indebted to Prof. Beric Skews of the University of the Witwatersrand, who provided valuable advice at the beginning of the study. Finally, it is a pleasure to acknowledge the assistance of Mr. David Maclucas (University of the Witwatersrand), who participated in the first trials of this test series.

References

Baird JP (1987) Supersonic vortex rings. Proc R Soc Lond A 409:59–65
Brouillette M, Hébert C (1997) Propagation and interaction of shock-generated vortices. Fluid Dyn Res 21:159–169
Chang SM, Chang KS (2000) Visualization of shock–vortex interaction radiating acoustic waves. J Vis 3(3):221–228
Cords PH (1968) A high resolution, high sensitivity color schlieren method. SPIE J 6:85–88
Elder FK, de Haas N (1952) Experimental study of the formation of a vortex ring at the open end of a cylindrical shock tube. J Appl Phys 23:1065–1069
Etoh TG, Poggemann D, Ruckelshausen A, Theuwissen A, Kreider G, Folkerts H-O, Mutoh H, Kondo Y, Maruno H, Takubo K, Soya H, Takehara K, Okinaka T, Takano Y, Reisinger T, Lohmann C (2002) A CCD image sensor of 1 Mframes/s for continuous image capturing of 103 frames, In: Technical digest of international solid state circuit conference, IEEE 0-7803-7335-9/02, pp 45–48
Kainuma M, Havermann M, Sun M, Takayama K (2005) Effects of the shock tube open-end shape on vortex loops released from it. In: Proceedings of the 24th international symposium on shock waves, Springer, Beijing, 2004, pp 505–510
Kleine H (2001) Flow visualization. In: Ben-Dor G, Igra O, Elperin T (eds) Handbook of shock waves, vol 1, Chap 5.1. Academic Press, San Diego, pp 685–740
Kleine H, Settles GS (2008) The art of shock waves and their flowfields. Shock Waves J 17(5):291–307
Kleine H, Ritzerfeld E, Grönig H (2003) Shock wave diffraction at a ninety degree corner. CFD J 12(2):142–158
Kleine H, Ramasundara S, Fien A (2008) Density-sensitive flow visualization of three-dimensional flow fields. In: Proceedings of 13th international symposium on flow visualization (Nice), paper 112 (CD proceedings)
Merzkirch W (1987) Flow visualization, 2nd edn. Academic Press, Orlando
Minota T (1998) Shock/vortex interaction in a flow field behind a shock wave emitted from a shock tube. In: Takayama K, Jiang Z (eds) Proceedings of the 2nd international workshop on shock–vortex interaction, Tohoku University, Sendai, pp 149–160
Minota T, Nishida M, Lee MG (1997) Shock formation by compressible vortex ring impinging on a wall. Fluid Dyn Res 21:139–157
Oertel H (1966) Stossrohre. Springer, Wien, pp 713–722
Ohtake H, Hayashida T, Kitamura K, Arai T, Yonai J, Tanioka K, Maruyama H, Etoh TG (2006) 300,000-pixel ultrahigh-speed high-sensitivity CCD and single-chip color camera mounting this CCD, NHK Broadcast Technology no. 28
Settles GS (2001) Schlieren and shadowgraph techniques. Springer, New York
Skews BW (1967) The perturbed region behind a diffracting shock wave. J Fluid Mech 29(4):705–719
Sun M, Takayama K (1997) The formation of a secondary shock wave behind a shock wave diffracting at a convex corner. Shock Waves J 7(5):287–295